A Reexamination of Hydrotalcite Crystal Chemistry

ARTICLE *in* THE JOURNAL OF PHYSICAL CHEMISTRY B · MAY 1996

Impact Factor: 3.3 · DOI: 10.1021/jp960039j

A Reexamination of Hydrotalcite Crystal Chemistry

Maurizio Bellotto, Bernadette Rebours,* Olivier Clause, and John Lynch

Institut Français du Pétrole, B.P. 311, 92506 Rueil Malmaison Cedex, France

Dominique Bazin and Eric Elkaïm

LURE, Bat. 209D, Centre Universitaire Paris-Sud, 91405 Orsay, France

Received: January 2, 1996[⊗]

The crystal chemistry of hydrotalcite-like compounds is investigated by powder diffraction methods such as Rietveld structure refinement, radial distribution function analysis, atom-specific radial distribution analysis obtained from anomalous diffraction data, and EXAFS spectroscopy. The topology of the brucite-type layer as well as the layer stacking arrangement and the intralayer bonding are determined for Mg,Al, Mg,Ga, and Ni,Al systems. The occurrence of long-range cation ordering in materials with M(II)/M(III) cation ratios close to 2.0 is observed only for systems with similar cation radii, and it is associated with a corrugation of the octahedral layer. The lack of ordering for systems with highly different cation radii is ascribed to the layer compression exhibited by these compounds, which prevents the layer distortion. The stacking arrangement is random for the solids investigated, except for the Mg,Al system which shows a preference for the rhombohedral polytype. It is proposed that this behavior is related to the extent of local directional bonds between the oppositely charged layers.

Introduction

This is the first of two papers dedicated to hydrotalcite (HT) and hydrotalcite-like compounds (HTlcs). This one will deal with their crystal chemistry and the second one [*J. Phys. Chem.* **1996**, *100*, 8535] with the thermal decomposition mechanisms yielding mixed oxides from the constituent cations. The interest of the authors in HTlcs was prompted by the use of the decomposed materials as catalysts or catalyst support, possibly after an activation−reduction step. Catalytic applications have been reported for a wide range of reactions, namely, basic catalysis, reforming, hydrogenation, oxidation, and Ziegler−Natta (for a review see ref 1). HTlcs are frequently formed during the synthesis of mixed oxide catalysts via the coprecipitation route. Evidence is also being gained about the formation of surface HTlcs during the impregnation of γ-Al_2O_3 with bivalent cations at pH values close to the isoelectric point of alumina.[2]

The structure of HTlc's was first elucidated by Allmann[3,4] for the CO_3−Mg,Fe system (pyroaurite and sjögrenite) and by Brown et al.[5,6] for the CO_3−Mg,Al system (hydrotalcite and manasseite). It can be visualised as made of brucite-type octahedral layers, in which M(III) cations partially substitute for M(II) cations. The positive charge of the octahedral layers resulting from this substitution is balanced by anions arranged in layers alternating with the octahedral ones. These interlayers are built from anions and water molecules to fill up all available sites. The stacking of the repeat units constituted by an octahedral layer and an interlayer can be arranged in two different ways, giving rise to two polytypes for each chemical composition. The one (e.g., pyroaurite and hydrotalcite) has a rhombohedral unit cell containing three stacked repeat units; the other (e.g., sjögrenite and manasseite) has a hexagonal unit cell containing two stacked repeat units. The local topology of the layer−interlayer bonding is the same for the two polytypes, the difference being confined to the long-distance layer−layer interactions.

The comprehension of HTlcs properties, as well as of the structure and reactivity of the decomposed and reduced products used as catalysts, requires understanding of their crystal chemistry. This is complicated by the extreme compositional variability exhibited by HTlcs,[7−9] which can be constituted by a wide variety of M(II),M(III) cation pairs, as well as by M(I),M(III) (e.g., Li,Al), M(II),M(IV) (e.g., Co,Si and Co,Ti), M(II),M(II) (e.g., Co,Zn and Ni,Zn) M(III),M(III) (e.g., La,Al), and M(IV),M(III) (e.g., V,Fe) cation pairs, and which can host different anions in the interlayer region, inorganic (e.g., CO_3^{2-}, NO_3^-, SO_4^{2-}, X^-, OH^-) as well as organic. The mineral chlorite itself can be considered as a HTlc in which the anion is $[Mg_3(Si_3Al)O_{10}(OH)_2]^-$.

Studies of the crystal chemistry of HTlcs have mainly dealt with the influence of composition on lattice parameters and on physical properties such as adsorption of probe molecules and anion exchange capacities.[10−13] The nature of the layer−interlayer bonding has been addressed by means of IR measurements of the vibrational frequencies of both the hydroxyls and the anions,[7,14−16] while the thermal behavior of the HTlcs has been studied by thermal analysis and X-ray diffraction.[12,16,17] However, the presence of faults in the stacking of successive layers, which is routinely observed in synthetic materials to depend on composition and preparation techniques,[18,19] has only been mentioned. When considering the structure of HTlcs, the presence of stacking faults is expected to be influenced by the nature of the layer−interlayer bonding as well as by the degree of hydrogen bonding. Similarly, the presence of long-range cation ordering is still a matter of debate.[20] Even if ordering should always occur according to the cation avoidance rule,[21] it is not routinely experimentally observed by powder XRD, except in the Li,Al system.[14,15] The small particle size of most of the samples, as well as the similar scattering power of Mg and Al, has been claimed responsible for the absence of clear-cut evidence of ordering for hydrotalcite. However, ordering is not observed even in the Ni,Al system[16] where the difference in scattering power between the cations should enable its experimental detection.

* To whom correspondence should be addressed.

[⊗] Abstract published in *Advance ACS Abstracts,* April 1, 1996.

S0022-3654(96)00039-1 CCC: $12.00

The aim of this paper is to investigate HTlcs crystal chemistry, which in turn will help the understanding of their thermal decomposition reaction path and of the structure and properties of the obtained mixed oxides. In the following we will be concerned mainly with the CO_3−Mg,Al system. To enhance the diffraction contrast between the M(II) and the M(III) cations, Ga has been substituted for Al in some samples. The Mg,Ga system is therefore considered as a model for the Mg,Al compounds. Reference will also be made to the Ni,Al system.

Experimental Section

Preparation and Chemical Analysis. The preparation of hydrotalcite-like materials has been reported elsewhere (refs 19 and 22 for Ni,Al; ref 23 for Mg,Al and Ga,Al). The coprecipitation method was adopted, at constant pH (pH = 8 for Ni,Al and pH = 9 for Mg,Al and Mg,Ga) and at a high supersaturation level, from the nitrate salts of the cations. The precipitation was carried out in a slight excess of sodium bicarbonate, and no precaution was taken to avoid contact with atmospheric CO_2; consequently, some carbonate ions were introduced in all the samples depending on their CO_3^{2-} affinity. The precipitates were kept in suspension at 333 K for half an hour under energetic stirring and then filtered and washed with distilled water until Na contents lower than 50 μg of Na per gram of sample were reached. The products were then dried for 16 h at 373 K. Part of the dried precipitates was subjected to a further hydrothermal treatment in distilled water (470 K, 2.5 MPa, 48 h) using a PTFE-covered glass-free autoclave in order to prevent contamination and formation of silicates.

The cation composition of the samples was checked by atomic absorption (Mg,Al and Ni,Al samples) using a Perkin-Elmer Model 360 spectrophotometer and by X-ray fluorescence (Mg,Ga samples) using a Philips PW1480 spectrometer. The amounts of C, N, and H were determined by gas chromatography of the gases evolved on combustion. The analysis was performed according to ASTM D 5291−92, standard method C, with the instrument Carlo Erba 1106.

X-ray Diffraction and Radial Distribution Function Analysis. X-ray diffraction powder patterns were measured using a Siemens D501 diffractometer in Bragg−Brentano reflection geometry, with Cu Kα radiation and a graphite diffracted beam monochromator. Structure refinement of the Mg,Al samples was performed with the GSAS Rietveld program.[24] The electron radial distribution function (RDF) was calculated for selected samples from the Fourier transform of the diffracted intensity data registered with a Siemens D500 diffractometer in symmetric transmission geometry. The Mo Kα_1 radiation was selected by a focusing quartz single-crystal incident beam monochromator. The sample was pressed to form a self-sustaining pellet, avoiding any holder in the beam path. The Q range explored was 0.15−15.00 Å^{-1}. The data were scaled to electron units according to the high angle method, after subtraction of air scattering and correction for absorption and polarization (for a review see ref 25). The WKM approximation[26] was used for the average scattering factor per electron. The use of symmetrical reflection geometry is particularly suited to RDF analysis because (a) the instrumental background is virtually zero, even in the low angle region ($1° \leq 2\theta \leq 5°$), (b) the sample absorption can be experimentally measured, which greatly simplifies the absorption correction, and (c) no effects of sample surface roughness modify the scattered intensity. The energy discrimination of the scintillation counter was carefully set in order to reject Ga fluorescence induced by Mo radiation.

EXAFS and Anomalous Diffraction. The chemical environment of Ga in Mg,Ga samples was investigated by extended X-ray absorption fine structure (EXAFS) and anomalous diffraction experiments. Both were performed at the LURE synchrotron facility in Orsay, using the radiation from the DCI storage ring running at 1.85 GeV with an average current of 300 mA. The EXAFS experiments were carried out on bending magnet line D44 in transmission mode at liquid N_2 temperature. A double-crystal Si (111) monochromator scanned the energy in 2 eV steps from 100 eV below to 900 eV above the Ga K absorption edge. Two ionization chambers were used as detectors. The sample thickness was set in order to have edge jump heights μx between 0.8 and 1.2 for the samples and the reference compounds. A sample of β-Ga_2O_3 was used as a reference for Ga in both octahedral and tetrahedral coordination, and a 5% Ga-substituted ZSM5 zeolite was used for Ga in tetrahedral coordination. The analysis of the EXAFS data was performed following standard procedures for extraction of the signal and normalization to the edge absorption. Fourier transforms of the EXAFS spectra were made after multiplication of the signal by a k^3 factor over a 3−14 Å^{-1} Hanning window. The Hanning window was identical for the references and for the investigated systems. A constant energy shift of 3.5 eV was applied to all the spectra.

The anomalous diffraction experiments were performed on bending magnet line D23, equipped with a general purpose four-circle goniometer. The setup was in parallel-beam reflection geometry on an infinitely thick sample. The wavelength was selected by a horizontally focusing double-crystal Si (111) monochromator followed by two mirrors to reject the harmonics. Two diffraction patterns were collected on the sample Mg/Ga = 2.0 at energies 10 and 200 eV below the Ga K absorption edge, fixed at the inflection point measured on the sample itself. The Q range explored was 0.54−9.34 Å^{-1}. Care was taken to measure air scattering, and a silicon standard was used to calibrate the wavelength. The patterns were corrected for air scattering and scaled to electron units. The scaling factor for the data set collected far from the edge was obtained with the high angle method, as described above. The scaling factor for the data set collected close to the edge was then deduced from the scaling factor of the data set collected far from the edge by considering the influences on the scaling factor caused by the differences in both the Ga f' and the absorption coefficient. The Raman resonant scattering was then subtracted from the pattern collected close to the edge as a constant background, determined by equating the experimentally measured scaled intensities and the calculated total coherent and incoherent scattering at high angles. The largest uncertainty concerned the f' values, set to −3.5 and −9.5 e far and close to the edge, respectively. Such values were set to those calculated by the FPRIME program[27] for the respective distances from the edge. However, fine-tuning of the f' value close to edge was necessary in order to minimize RDF oscillations in the 0−1 Å region. This resulted in larger than calculated $\Delta f'$ values, a feature already observed experimentally[28] and not yet correctly explained. After appropriate intensity scaling the data can be subtracted, to obtain the differential anomalous scattering (DAS), and Fourier transformed to yield the Ga environmental RDF.[29,30] Alternatively, the total RDF may be calculated by Fourier transform of each data set. The subtraction of the total RDFs yields the Ga environmental RDF or differential RDF (DRDF). The authors believe that the second approach gives a better control over all the steps of data treatment. The experimental DRDF must be scaled to the $\Delta f''$ contribution relative to the average total electron density of the compound in order to yield the atom-specific electron density distribution function $D_i(r)$ which can be compared to the calculated one for a specific structure.

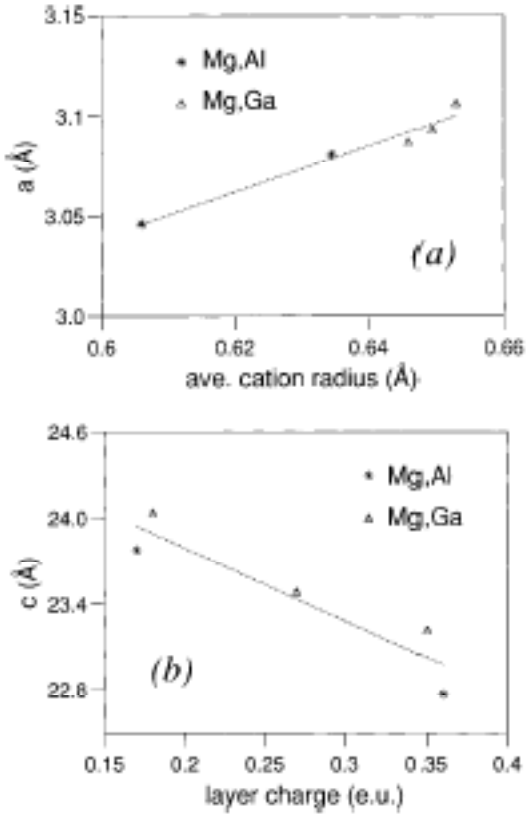

Figure 1. Correlations between lattice parameters and composition for Mg,Al and Mg,Ga HTlcs: (a) a vs average cation ionic radius, (b) c vs layer charge.

TABLE 1: Sample Composition

sample	nominal composition	chemical formula
1	Mg/Al = 2.0	$[Mg_{0.64}Al_{0.36}(OH)_2](CO_3)_{0.18}{\cdot}0.46H_2O$
2	Mg/Al = 5.0	$[Mg_{0.83}Al_{0.17}(OH)_2](CO_3)_{0.08}{\cdot}0.75H_2O$
3	Mg/Ga = 2.0	$[Mg_{0.65}Ga_{0.35}(OH)_2](CO_3)_{0.07}(NO_3)_{0.20}{\cdot}0.19H_2O$
4	Mg/Ga = 2.5	$[Mg_{0.75}Ga_{0.25}(OH)_2](CO_3)_{0.10}(NO_3)_{0.07}{\cdot}0.49H_2O$
5	Mg/Ga = 5.0	$[Mg_{0.82}Ga_{0.18}(OH)_2](CO_3)_{0.01}(NO_3)_{0.16}{\cdot}0.49H_2O$
6	Ni/Al = 2.5	$[Ni_{0.73}Al_{0.27}(OH)_2](CO_3)_{0.12}(NO_3)_{0.03}{\cdot}0.55H_2O$

Results

Chemical Composition and Structural Arrangement. The chemical compositions of the samples investigated are reported in Table 1. In the following the samples will be named according to their nominal cation composition; i.e., sample 1 will be named Mg/Al = 2.0. The samples Mg/Ga = 2.5 and Ni/Al = 2.5 have been submitted to hydrothermal treatment, and the hydrotreated samples will be referred to as Mg/Ga = 2.5 H and Ni/Al = 2.5 H. It is apparent that Mg,Al samples have been completely CO_3^{2-} substituted, while substantial amounts of NO_3^- ions still remain in the Mg,Ga and Ni,Al samples. The lattice parameters of the Mg,Al and Mg,Ga samples can be related to the average cation radius (a parameter) and to the octahedral layer charge (c parameter), as shown in Figure 1.

The X-ray powder diffraction patterns of samples Mg/Al = 2.0, Mg/Ga = 2.5, and Ni/Al = 2.5 are shown in Figure 2. The Mg,Al sample exhibits a better crystallinity and virtually no stacking faults, as evidenced by the sharpness and symmetry of the (01l) reflections. On the contrary, the Mg,Ga and Ni,Al samples exhibit a high stacking fault density which is not affected by the hydrothermal treatment, as evidenced in Figure 3 by the comparison of the XRD patterns of Mg/Ga = 2.5 and Mg/Ga = 2.5 H and of Ni/Al = 2.5 and Ni/Al = 2.5 H. The hydrothermal treatment increases the crystallinity of the samples

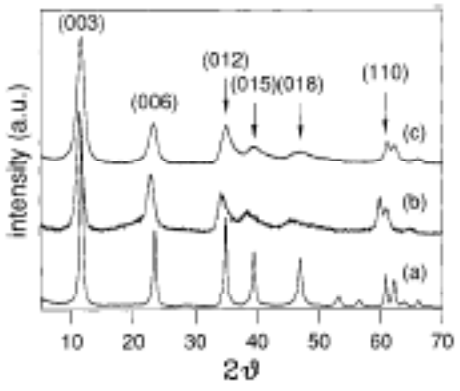

Figure 2. X-ray powder diffraction patterns of (a) Mg/Al = 2.0, (b) Mg/Ga = 2.5, and (c) Ni/Al = 2.5.

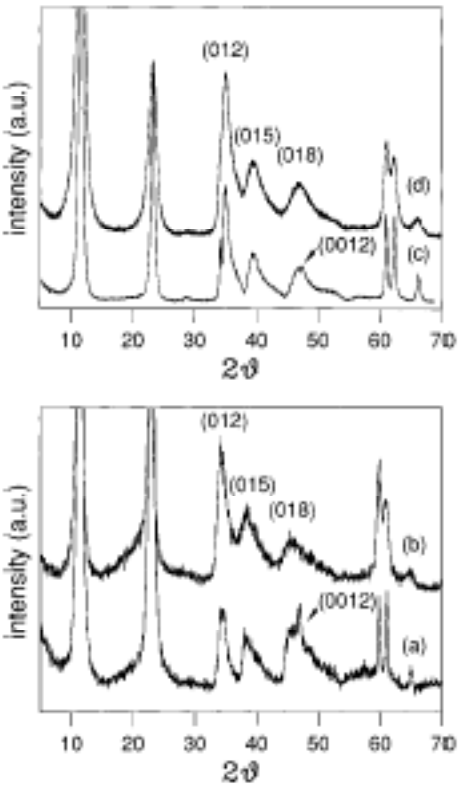

Figure 3. X-ray powder diffraction patterns of (a) Mg/Ga = 2.5 H, (b) Mg/Ga = 2.5, (c) Ni/Al = 2.5 H, and (d) Ni/Al = 2.5. Note the appearance of the (0012) basal reflection in the hydrotreated samples.

but does not alter the stacking arrangement. Cation ordering is evident in sample Mg/Ga = 2.0 as indicated by the reflection at $d \cong 4.63$ Å shown in Figure 4; compare the XRD patterns of Mg/Ga = 2.0 and Mg/Ga = 2.5. It can also be observed that the (01l) reflections, and in particular the (015), are shifted toward low 2θ values in sample Mg/Ga = 2.0. This shift cannot be explained by differences in lattice parameters, which would show up in the basal reflections (c value) and in the (110) reflection (a value) and thus must be due to differences in the stacking arrangement.

Structure Refinement of the Mg,Al Samples. The absence of stacking faults in the Mg,Al samples enabled the Rietveld refinement of their structure. Samples Mg/Al = 2.0 and Mg/Al = 5.0 were refined with space group $R\bar{3}m$, as reported in the literature for the rhombohedral polytype of hydrotalcite.[31] In the case of Mg/Al = 2.0 the possible presence of cation ordering was checked, by trying to refine its structure also with space group $P3_1$. The presence of different Mg−OH and Al−OH bond lengths should indeed reduce the symmetry of samples

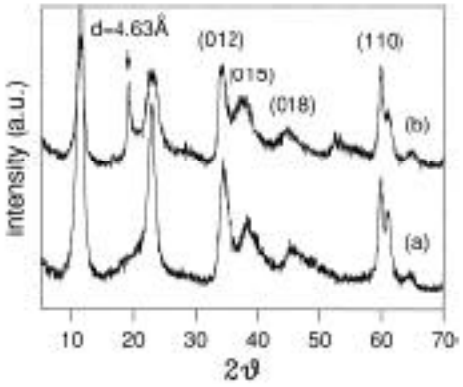

Figure 4. X-ray powder diffraction patterns of (a) Mg/Ga = 2.5 and (b) Mg/Ga = 2.0.

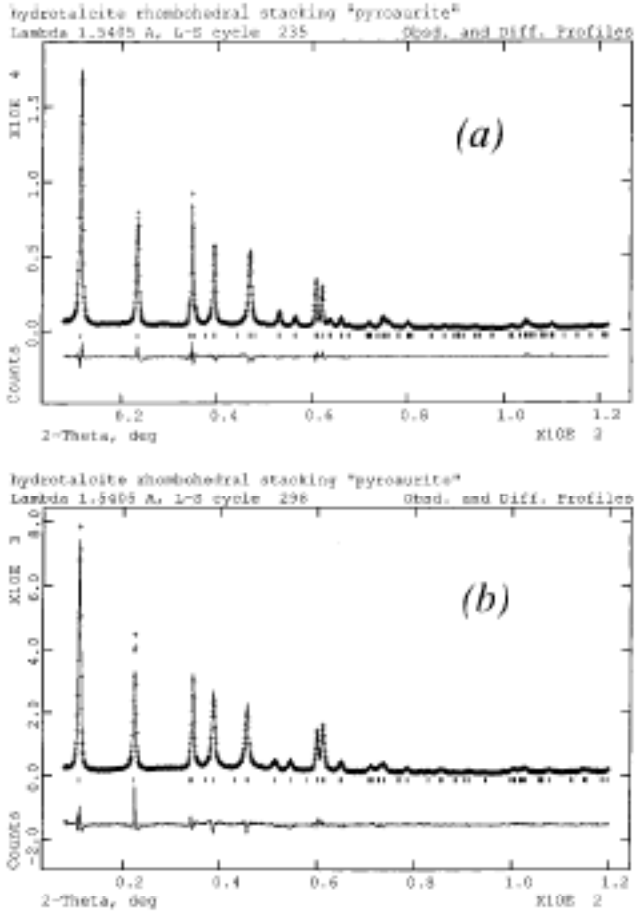

Figure 5. Experimental, calculated, and difference X-ray powder diffraction patterns for (a) Mg/Al = 2.0 and (b) Mg/Al = 5.0.

with a 2:1 cation ratio.[20] No improvement in the statistical indices was observed, as compared to the refinement carried out with space group $R\bar{3}m$, but convergence problems showed up even in the presence of strong soft constraints on the interatomic distances. The experimental, calculated, and difference diffraction patterns are shown in Figure 5 for Mg/Al = 2.0 and Mg/Al = 5.0. The refinement results and atomic positions are reported in Table 2 while the interatomic distances are reported in Table 3. The site occupancies have been fixed according to the nominal composition, a single atomic displacement factor has been refined for the cations and a different one for C, H(1), and H(2), and finally O(2), C, and H(2) have been constrained to the $z = 0.5$ plane. It should be remarked that the introduction of hydrogen, contributing to the interlayer electronic density, is essential to approach the correct ratio between the basal reflection intensities, even though some

TABLE 2: Rietveld Refinement Results

sample	Mg/Al = 2.0	Mg/Al = 5.0
space group	$R3m$	$R3m$
lattice parameters	$a = 3.0460(1)$ Å	$a = 3.0808(3)$ Å
	$c = 22.772(2)$ Å	$c = 23.784(4)$ Å
preferred orientation	$m = 1.000(2)$	$m = 1.041(4)$
statistical indices	$R_{wp} = 0.0893$	$R_{wp} = 0.1174$
	$\chi^2 = 4.2$	$\chi^2 = 4.7$

Atomic Positions Mg/Al = 2.0

atom	x	y	z	$100U$	site	occupancy
Mg	0.0	0.0	0.0	2.27(5)	3a	2/3
Al	0.0	0.0	0.0	2.27(5)	3a	1/3
O(1)	0.0	0.0	0.37634(9)	3.85(8)	6c	1
H(1)	0.0	0.0	0.418(1)	8.4(7)	6c	1
O(2)	0.1058(7)	−0.1058(7)	0.5	2.9(2)	18h	1/6
C	1/3	2/3	0.5	8.4(7)	6c	1/12
H(2)	1/3	2/3	0.5	8.4(7)	6c	1/2

Atomic Positions Mg/Al = 5.0

atom	x	y	z	$100U$	site	occupancy
Mg	0.0	0.0	0.0	3.19(8)	3a	5/6
Al	0.0	0.0	0.0	3.19(8)	3a	1/6
O(1)	0.0	0.0	0.3754(2)	3.6(1)	6c	1
H(1)	0.0	0.0	0.432(1)	5.9(7)	6c	1
O(2)	0.1260(9)	−0.1269(9)	0.5	2.1(3)	18h	1/6
C	1/3	2/3	0.5	5.9(7)	6c	1/24
H(2)	1/3	2/3	0.5	5.9(7)	6c	3/4

TABLE 3: Interatomic Distances (Å) and Angles (deg)

distances	Mg/Al = 2.0	Mg/Al = 5.0
(Mg,Al)−OH	2.013(1)	2.040(2)
$(OH-OH)_{\text{shared edges}}$	2.632(3)	2.676(5)
$(O-OH)_{\text{layer-interlayer}}$	2.871(2)	3.040(4)
$(O-OH)_{\text{interlayer-interlayer}}$	2.696(1)	2.694(1)
C−O	1.200(4)	1.106(5)
layer thickness	1.9587	2.0010
interlayer thickness	5.6320	5.9270
angles	**Mg/Al = 2.0**	**Mg/Al = 5.0**
OH−(Mg,Al)−OH	98.33(6)	98.1(1)
OH−(Mg,Al)−OH	81.67(6)	82.0(1)
O−C−O	120	120

discrepancies can still be observed for Mg/Al = 5.0. The cation−hydroxyl distance decreases with increasing Al content, as expected from the cation radii values. The octahedra are distorted, being flattened and extended approximately in the same degree for the two samples, as indicated by the OH−(Mg,Al)−OH bond angles. The flattening of the octahedra brings about very short OH−OH distances in the shared octahedral edges. The interlayer compression accounts virtually for the entire basal spacing contraction on increasing Al concentration. This reflects in the strengthening of the hydrogen bonds between the layer and the interlayer, as already observed by IR spectroscopy by Miyata and Hernandez-Moreno et al.[7,32] On the contrary, the hydrogen bonds within the interlayer are virtually independent of Al content. The C−O distances in CO_3^{2-} groups are much shorter than the value of 1.283 Å for calcite, but they are certainly poorly determined because the structural model is incorrect since no effort was made to account for disorder in the interlayer. Similarly, the H(1) site is expected to be poorly determined, and no speculation can be inferred from the O(1)−H(1) distance.

Structure Determination of the Faulted Samples. The other samples show stacking faults in the broad and asymmetric (01*l*) reflections. The faults are a result of the intergrowth of the rhombohedral and hexagonal polytypes. The powder X-ray diffraction pattern of sample Mg/Ga = 5.0 has been simulated with the DIFFAX program, which enables modeling of extended planar faults with a statistical recursive approach.[33] The

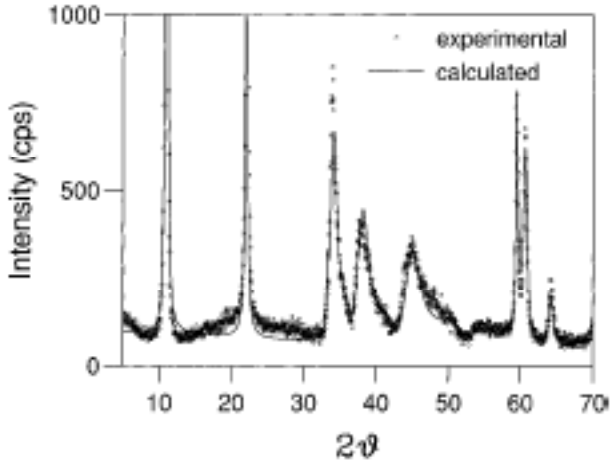

Figure 6. Experimental and calculated X-ray powder diffraction patterns for sample Mg/Ga = 5.0.

occurrence of faults has been quantified by a "fault probability" (FP) which describes the probability for a specific layer sequence to be arranged in rhombohedral or hexagonal stacking. A value of FP = 1.0 describes the pure rhombohedral polytype and FP = 0.0 the pure hexagonal polytype, while a value of FP = 0.5 describes a random layer sequence. The best agreement between the experimental and calculated profiles has been obtained for FP = 0.6 and is shown in Figure 6. The statistical agreement factor between the profiles is $R_{wp} = 0.19$. The other Mg,Ga and Ni,Al samples exhibit a similar behavior, except Mg/Ga = 2.0, which presents cation ordering leading to an $a\sqrt{3}$ superstructure in the octahedral plane. In this case also a simulation of the powder patten has been performed with the DIFFAX program. The superstructure cell contains three random cells, and the stacking can be arranged in such a way that the origin is located above the origin of each of the three random cells. The origins of the superstructure cells of neighboring layers show no correlation, the superstructure being completely disordered along the *c* axis. Moreover, the stacking sequence is different in this sample as the cations of successive layers are never superimposed as in the hexagonal stacking but may occupy either sites shifted by 2*a*/3,*b*/3 as in the regular rhombohedral stacking or sites shifted by *a*/3,2*b*/3. In the usual notation of layer packing we may say that if A are the sites occupied in a layer, in the successive layer the sites occupied are either the B sites as in the regular rhombohedral stacking or the C sites. In the latter case the OH groups around the interlayer are no longer superimposed, as is the case in both the rhombohedral and hexagonal stacking, but are shifted by either 2*a*/3,*b*/3 or *a*/3,2*b*/3; i.e., they are superimposed as in a compact stacking. The two stacking types are illustrated in Figure 7, while the experimental and simulated profiles are reported in Figure 8. The statistical agreement factor between the profiles is $R_{wp} = 0.17$. The stacking sequence described involves only minor modifications in the layer−interlayer bonding and in the hydrogen bond lengths.

The presence of a high stacking fault density precludes the possibility of performing Rietveld−type structural refinements on the Mg,Ga samples. Therefore, to get information on the local structure, we resorted to the RDF analysis. The total RDF obtained from laboratory data gives a weighted electron density distribution function described by

$$\rho(r) = \sum_i x_i D_i(r)$$

where x_i is the fraction of electron density contributed by atom *i* in the compound and $D_i(r)$ is the electron density distribution

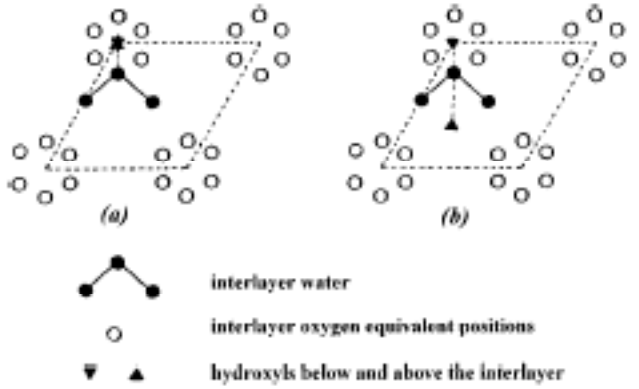

Figure 7. Projection on the basal plane of (a) the normal layer−interlayer configuration and (b) the configuration determined by the different stacking arrangement of sample Mg/Ga = 2.0.

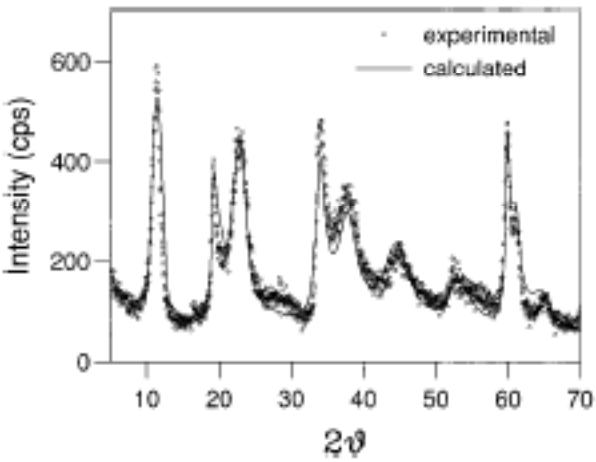

Figure 8. Experimental and calculated X-ray powder diffraction patterns for sample Mg/Ga = 2.0.

around atom *i*. The comparison of the oscillating part of the RDF, i.e., $\rho(r) - \rho_0$ where ρ_0 is the average electron density of the material, is shown in Figure 9 for the Mg,Al and Mg,Ga samples. The RDF of the samples with a cation ratio of 5.0 compare well, considering the higher electron density of Ga with respect to Al which accounts for the higher intensity of the maxima at about 3.0 Å (first cation−cation distance) and at about 5.3 Å (second cation−cation distance). These maxima show the difference in the *a* lattice parameter between the samples (Mg,Al = 3.081 Å, Mg,Ga = 3.106 Å). The shift of the peaks at $r \geq 7.5$ Å implies a difference in thickness of the basic layer plus interlayer unit (Mg,Al = 7.928 Å, Mg,Ga = 8.011 Å) and a difference in the stacking arrangement. Moreover, the cation−oxygen distance is very close for the two samples. The RDF of the samples with a cation ratio of 2.0 show differences due to the cation ordering pattern of the Mg,Ga sample. The second cation−cation distance at about 5.3 Å is much higher since it corresponds to Ga−Ga only. A difference in thickness of the layers (Mg,Al = 7.591 Å, Mg,Ga = 7.737 Å) and stacking sequence is observed at $r \geq 7.5$ Å. It should be remarked that the Mg,Ga sample shows a shorter cation−oxygen distance at about 2.0 Å and longer cation−cation distances at about 3.0 and 5.3 Å which cannot entirely be explained by the larger *a* cell parameter (Mg,Al = 3.046 Å, Mg,Ga = 3.087 Å). A summary of interatomic distances obtained by the RDFs and by Rietveld and lattice parameter determination is presented in Table 4.

Local Ga Environment in the Mg,Ga Samples. Much more detailed information on the local Ga environment is given by the Ga environmental RDF, $D_{Ga}(r)$, obtained from anomalous diffraction experiments as described in the Experimental Section.

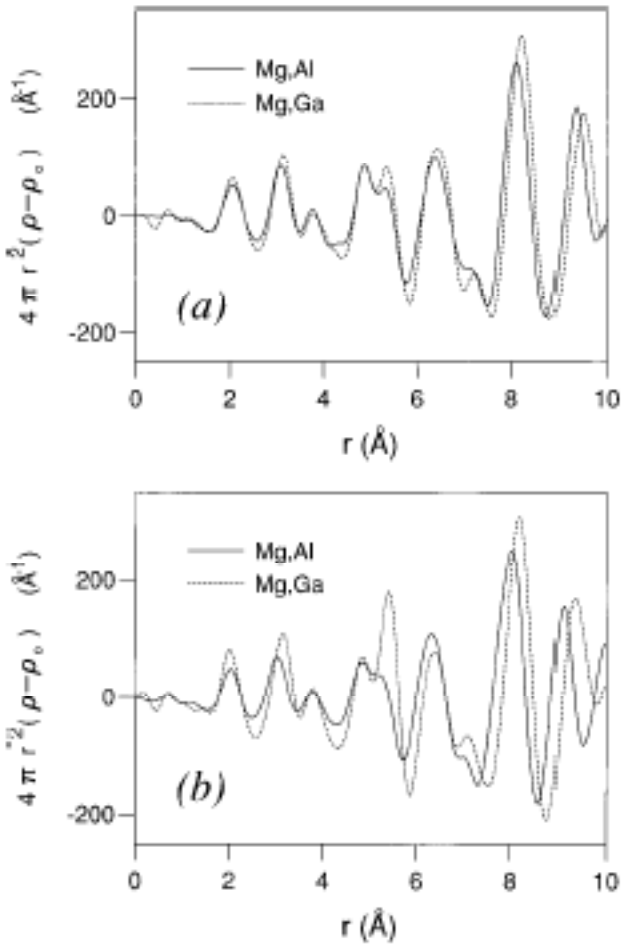

Figure 9. Radial distribution functions for (a) Mg/Al = 5.0, Mg/Ga = 5.0 and (b) Mg/Al = 2.0, Mg/Ga = 2.0.

TABLE 4: Interatomic Distances (Å) from RDF and Rietveld or Lattice Parameters

sample Mg/Al = 5.0	RDF	Rietveld
(Mg,Al)−O	2.05(1)	2.040(2)
cation−cation 1st distance	3.08(1)	3.0808(3)
cation−cation 2nd distance	5.33(1)	5.3361(5)
sample Mg/Al = 2.0	RDF	Rietveld
(Mg,Al)−O	2.03(1)	2.013(1)
cation−cation 1st distance	3.04(1)	3.0460(1)
cation−cation 2nd distance	5.26(1)	5.2758(2)
sample Mg/Ga = 5.0	RDF	lattice parameters
(Mg,Ga)−O	2.05(1)	
cation−cation 1st distance	3.11(1)	3.106(5)
cation−cation 2nd distance	5.37(1)	5.38(1)
sample Mg/Ga = 2.0	RDF	lattice parameters
(Mg,Ga)−O	2.02(1)	
cation−cation 1st distance	3.14(1)	3.087(5)
cation−cation 2nd distance	5.41(1)	5.35(1)

To examine in detail the local distortions induced by cation ordering, the distribution function $D_{Ga}(r)$ for sample Mg/Ga = 2.0 has been obtained. It is shown in Figure 10 along with the $D_{Ga}(r)$ calculated for a hydrotalcite structure of the observed lattice parameters and with an average Ga−O distance as determined by the total RDF. It can be observed that the Ga−O distance is shorter than the average cation−oxygen distance. On the contrary, the cation−cation distances, Ga−Mg at about 3.0 Å, Ga−Ga at about 5.3 Å, and Ga−Mg at about 6.1 Å, are larger than calculated. It appears that the cation ordering pattern induces a distortion of the octahedral layer, causing different Mg−O and Ga−O distances. Within each octahedron the cation−oxygen distances must therefore no longer be equal.

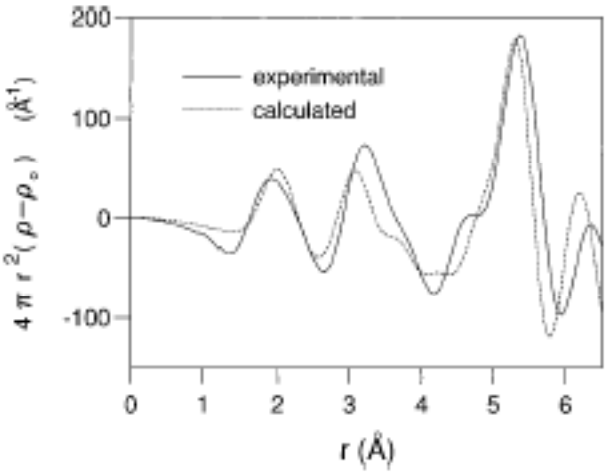

Figure 10. Experimental and calculated Ga environmental radial distribution functions for Mg/Ga = 2.0.

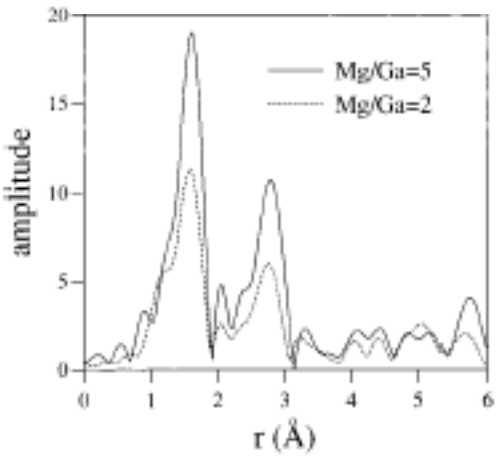

Figure 11. EXAFS Fourier transform moduli for Mg/Ga = 5.0 and Mg/Ga = 2.0, ex situ, room temperature.

Moreover, the discrepancy between the lattice parameter values and the cation−cation distances are only compatible with a corrugation of the octahedral layers which lose their planarity. Detailed local characterization of the Ga environment is also obtained by EXAFS spectroscopy, but in this case the information is limited to the first and second coordination shells. The modulus of the Fourier transform of the EXAFS signal for samples Mg/Ga = 5.0 and Mg/Ga = 2.0 is shown in Figure 11. It is apparent that the amplitude is lower for sample Mg/Ga = 2.0, thus pointing to the presence of static disorder in this sample. The Ga−O coordination number is fixed at 6 as proven by the RDF and DRDF data. This result confirms the distortion of the coordination octahedra as a result of cation ordering. The distances (r), coordination numbers (cn), and Debye−Waller factors (σ) determined by EXAFS are reported in Table 5 along with the distances determined by DRDF. In order to check that the difference between the amplitudes of the first-shell EXAFS moduli for samples Mg/Ga = 5.0 and Mg/Ga = 2.0 is due to a deformation of the coordination octahedra and to the appearance of two different Ga−O distances in Mg/Ga = 2.0, an effort was made in the latter case to fit the EXAFS signal with two different distances and with a fixed Debye−Waller factor equal to the one obtained for Mg/Ga = 5.0. The following values were obtained: $r_1 = 1.94$ Å, $cn_1 = 3.2$, $r_2 = 2.05$ Å, $cn_2 = 2.6$, and $\sigma_1 = \sigma_2 = 0.06$ Å. These values were compared with those obtained by fitting a single distance and reported in Table 5: $r = 1.98$ Å, cn = 6.0, and $\sigma = 0.09$ Å.

TABLE 5: Ga Environment[a]

sample Mg/Ga = 5.0 from EXAFS	1st shell (Ga−O) r = 1.99(2) Å cn = 6.0 σ = 0.06(2) Å	2nd shell (Ga−Mg) r = 3.16(3) Å cn = 6.0 σ = 0.06(3) Å
sample Mg/Ga = 2.0 from EXAFS	1st shell (Ga−O) r = 1.98(3) Å cn = 6.0 σ = 0.09(2) Å	2nd shell (Ga−Mg) r = 3.13(5) Å cn = 6.0 σ = 0.08(4) Å
sample Mg/Ga = 2.0 from anomalous diffraction	1st shell (Ga−O) r = 1.95(1) Å	2nd shell (Ga−Mg) r = 3.20(1) Å

[a] cn = coordination number.

Discussion

Cation Ordering in M(II)/M(III) Samples. The structure of HTlcs is built up from octahedral brucite-type layers. Such layers are compressed along the c axis and expanded along the plane, a feature that is found also in brucite where the Mg−Mg repulsion extends the b axis to 9.43 Å (with reference to the conventional axes definition of the dioctahedral and trioctahedral minerals; for brucite and HTlcs b axis = $3a$), greater than for almost all other trioctahedral layer silicates. The compression of the layer is limited by the close approach of oxygen atoms along shared octahedral edges. In brucite the OH−OH distance is 2.785 Å, and the layer thickness is 2.113 Å.[34] A similar behavior is exhibited by gibbsite, where the average OH−OH distance between shared edges of occupied and unoccupied octahedra is 2.635 Å (gibbsite is dioctahedral) and the layer thickness is 2.050 Å.[35] When trioctahedral minerals such as HTlcs contain M(II) and M(III) cations with a ratio close to 2, ordering is commonly found in the literature, a feature which tends to minimize cation−cation repulsion across shared octahedral edges and which is formally described in the cation avoidance rule.[21] Such ordering goes along with a counter rotation of the upper and lower oxygen octahedral triads in order to shorten the shared edges and shield the cations from each other. The consequent distortion of the octahedral layer accommodates different cation−oxygen bond lengths. Long-range ordering is not commonly observed in HTlcs, even though evidence of local ordering is provided by IR spectroscopy.[32] Long-range order is found only in Li,Al[14,15] and Mg,Ga systems, and thus it seems to be dependent on the cation composition of the material. The ordering pattern of HTlcs which implies the lack of cation segregation is of crucial practical importance, since these materials are used as cation sources to obtain, upon decomposition, mixed oxides with a good level of homogeneity in the cation distribution.

To unravel this peculiarity of HTlcs, it must be recognized that the octahedral layer compression in these compounds is higher than that observed in brucite and gibbsite. The Rietveld structure refinements show that for Mg/Al = 5.0 the layer thickness is 2.001 Å, while for Mg/Al = 2.0 the layer thickness is 1.959 Å. Consequently, the OH−OH distance across shared octahedral edges, 2.676 Å for Mg/Al = 5.0 and 2.632 Å for Mg/Al = 2.0, has already attained its minimum value. The absence of long-range order in Mg/Al = 2.0 is shown by the failure of the powder diffraction pattern Rietveld refinement with space group $P3_1$. It comes from the already close OH−OH approach, which prevents the layer distortions brought about by the ordering process. The ordering in Li,Al systems is readily explained by considering that Li occupies the vacant expanded sites in a dioctahedral gibbsite-type layer. In M(II),M(III) HTlcs ordering can happen only with cations of similar ionic radius, as for Mg/Ga = 2.0. In such a case the ordering can proceed without major distortions of the octahedra and thus without major distortions of the octahedra and thus without any further decrease of the OH−OH distance. Different Ga−O and Mg−O distances do appear as shown by the DRDF, EXAFS, and RDF data, and within each octahedron the cation−oxygen distances lie within a range and are no longer all equal, as shown by the EXAFS measurements. However, the values observed for such Ga−O and Mg−O distances, i.e., 1.95−1.98 and 2.02 Å, respectively, do not differ strongly, and ordering can proceed. The ordering process appears to provoke a corrugation of the layer, as suggested by the DRDF analysis. Such buckling of the octahedral layer increases the cation−cation distances, thus minimizing repulsion. In the case of Mg/Al = 2.0 the Al−O and Mg−O bond length difference should be much higher, e.g., 1.90 Å for Al−O in gibbsite and 2.11 Å for Mg−O in brucite; consequently, the distortion of the octahedra should also be larger, but this is prevented by the layer compression.

Layer Stacking. The layers in HTlcs can be stacked in such a way that the cations of neighboring octahedral sheets either are on the vertical of each other or are shifted by $2a/3,b/3$. These two stacking sequences, if extended throughout the crystal without faults, produce the two hexagonal and rhombohedral polytypes, respectively. The local topology of the layer−interlayer bonding is the same for the two arrangements, and only the long-range layer−layer interactions are different. Consequently, in most synthetic HTlcs the stacking arrangement is random. This is in fact the stacking arrangement that we have found for the Mg,Ga and Ni,Al systems, as proven by the good agreement between the simulated and experimental diffraction patterns. Only in the case of Mg/Ga = 2.0 does the layer corrugation bring about a different stacking type, where facing OH groups may not be superimposed as in both the rhombohedral and hexagonal polytypes. This arrangement, however, does not modify substantially the layer−interlayer hydrogen bonding because the interlayer oxygens are always shifted from the 3m position, which lies on the line connecting the OH groups for both the rhombohedral and hexagonal arrangement (i.e., they are in position 18h rather than 3b). For example in the Mg,Al samples the shift of the interlayer oxygens out of symmetry position is 0.558 and 0.672 Å for Mg/Al = 2.0 and Mg/Al = 5.0, respectively, and the different arrangement would cause an increase of the hydrogen-bonding distance of only 6.6% and 4.1%, respectively. It can be argued that the specific corrugated layer configuration of sample Mg/Ga = 2.0 further reduces the differences.

The disordered stacking arrangement is not influenced by hydrothermal treatment performed at 470 K. This is in line with the result of Pausch et al.,[18] who found that in CO_3^{2-}-free systems the formation of the rhombohedral polytype occurs upon hydrotreating at temperatures lower than 423 K, and with the observation of Allmann[4] that in the pyroaurite−sjögrenite CO_3−Mg,Fe system rhombohedral pyroaurite is the low-temperature polymorph because it is found in the outermost shell of natural crystals. These observations are also readily explained on the basis of entropy considerations.

The Mg,Al samples are somewhat different compared to the Mg,Ga and Ni,Al ones. They exhibit a well-organized rhombohedral stacking and show no traces of the nitrate ions used during the synthesis, which are still retained in different amounts in the others. Pausch et al.[18] already found that the presence of carbonate in Mg,Al HTlcs gives rise to a well-organized rhombohedral polytype, while Miyata[13] found that CO_3^{2-} is the most selective anion during anion exchange of Mg,Al systems. Therefore, it appears that Mg,Al hydrotalcites are sensitive to long-range interactions, and the charge balance is not entirely satisfied by the local intralayer bonding. Thus, the arrangement in which the cations belonging to neighboring layers are further

apart is favored. Moreover, the layer−interlayer bonding appears nondirectional, since anion exchange is easy and the selectivity is controlled only by the size of the anion.[13] These two observations point to the fact that the layer−interlayer bonding in Mg−Al HTlcs is essentially Coulombic without strong directional bonds. The presence of hydrogen bonding has been proven by IR spectroscopy, both between the octahedral layer and the anionic interlayer and within the interlayer between the water molecules and the anions. Nevertheless, the Al−OH distances in Mg/Al = 2.0 and Mg/Al = 5.0 are very long, 2.013 and 2.040 Å, respectively, as expected for no OH polarization and no hydrogen bonding for the Al-centered octahedra. This would explain the ease of anion exchange and the long-range cation repulsion, since the charge remains confined to the Al atoms.

Conclusions

Hydrotalcite-like compounds have an important industrial application as catalyst precursors. The materials obtained upon decomposition of HTlcs exhibit interesting properties of thermal stability which are likely connected to the cation distribution. In order to be able to control the decomposition process and to tailor the properties of the decomposed materials, it is necessary to get more insight in the crystal chemistry of the starting material. In particular, the important characteristics are the cation distribution within the octahedral layers and the nature of the intralayer bonding.

Cation ordering is expected in M(II),M(III) HTlcs with cation ratios close to 2, but it is not usually observed. This anomaly comes from the characteristics of the octahedral layer, which is compressed along the vertical and expanded along the plane even more than is found in brucite or gibbsite. This flattening of the octahedral layer results in short oxygen−oxygen distances along shared edges, which cannot sustain the further shortening brought about by the distortions connected with ordering. Ordering is observed only for cations of similar ionic radius, as Mg and Ga, since in such a case it can proceed without important octahedra distortions. In an ordered Mg/Ga = 2.0 sample the octahedral layer appears buckled, so as to increase the distance between the cations and minimize their repulsion. The average Mg−O and Ga−O distances, however, are not much different, as expected.

Most of synthetic samples show a random stacking sequence, which can be imagined as a very fine intergrowth of the two possible rhombohedral and hexagonal polytypes. This arrangement is expected on the basis of the equal layer−interlayer topology of the two polytypes. The stacking sequence is not affected by hydrothermal treatments performed at 470 K, which increase the crystallinity without affecting the layer sequence. The higher entropy of a random sequence accounts for its stability at a relatively high temperature. However, the Mg,Al system shows a marked preference for the rhombohedral stacking, in which the cations belonging to successive layers are further apart. This feature, together with the easier CO_3^{2-} ion exchange exhibited by these samples, points to a predominantly Coulombic layer−interlayer bonding. This interpretation is supported also by the observation of the long Al−OH distances in the octahedral layer which suggest no polarization of the OH and no hydrogen bonding of the Al−centered octahedra.

Acknowledgment. We express our thanks to the technical staff of LURE for the setup of the EXAFS and anomalous diffraction experiments. Stimulating discussions with Dr. Espinat and permission to use the software for RDF analysis are gratefully acknowledged.

References and Notes

(1) Cavani, F.; Trifirò, F.; Vaccari, A. *Catal. Today* **1991**, *11*, 173.
(2) Paulhiac, J. L.; Clause, O. *J. Am. Soc.* **1993**, *115*, 11602.
(3) Allmann, R.; Lohse, H. H. *Neues Jahrb. Mineral., Monatsh.* **1966**, 161.
(4) Allmann, R. *Acta Crystallogr.* **1968**, *B24*, 972.
(5) Gastuche, M. C.; Brown, G.; Mortland, M. *Clay Miner.* **1967**, *7*, 177.
(6) Brown, G.; Gastuche, M. C. *Clay Miner.* **1967**, *7*, 193.
(7) Miyata, S. *Clays Clay Miner.* **1975**, *23*, 369.
(8) Taylor, R. M. *Clay Miner.* **1984**, *19*, 591.
(9) Drits, V. A.; Sokolova, T. N.; Sikolova, G. V.; Cherkashin, V. I. *Clays Clay Miner.* **1987**, *35*, 401.
(10) Miyata, S.; Okada, A. *Clays Clay Miner.* **1977**, *25*, 14.
(11) Miyata, S.; Hirose, T. *Clays Clay Miner.* **1978**, *26*, 441.
(12) Miyata, S. *Clays Clay Miner.* **1980**, *28*, 50.
(13) Miyata, S. *Clays Clay Miner.* **1983**, *31*, 305.
(14) Sema, C. J.; White, J. L.; Hem, S. L. *Clays Clay Miner.* **1977**, *25*, 384.
(15) Sema, C. J.; Rendon, J. L.; Iglesias, J. E. *Clays Clay Miner.* **1982**, *30*, 180.
(16) Kruissink, E. C.; van Reijen, L. L.; Ross, J. R. H. *J. Chem. Soc., Faraday Trans. 1* **1981**, *77*, 649.
(17) Brindley, G. W.; Kikkawa, S. *Clays Clay Miner.* **1980**, *28*, 87.
(18) Pausch, I.; Lohse, H. H.; Schürmann, K.; Allmann, R. *Clays Clay Miner.* **1986**, *34*, 507.
(19) Clause, O.; Gazzano, M.; Trifirò, F.; Vaccari, A.; Zatorski, L. *Appl. Catal.* **1991**, *73*, 217.
(20) Hofmeister, W.; von Platen, H. *Cryst. Rev.* **1992**, *3*, 3.
(21) Radoslovich, E. W. *Am. Miner.* **1963**, *48*, 76.
(22) Clause, O.; Rebours, B.; Merlen, E.; Trifirò, F.; Vaccari, A. *J. Catal.* **1992**, *133*, 231.
(23) Rebours, B.; d'Espinose de la Caillerie, J. B.; Clause, O. *J. Am. Chem. Soc.* **1994**, *116*, 1707.
(24) Larson, A. C.; von Dreele, R. B. GSAS *Generalized Structure Analysis Package*, Document LAUR 86-748, Los Alamos National Laboratory.
(25) Mangini, M.; Licheri, G.; Piccaluga, G.; Paschina, G.; Pinna, G. *X-ray Diffraction of Ions in Aqueous Solutions: Hydration and Complex Formation*; CRC: Boca Raton, FL, 1988; Chapters 1, 2.
(26) Warren, B. E.; Krutter, H.; Morningstar, O. *J. Am. Ceram. Soc.* **1936**, *19*, 202.
(27) Cromer, D. L. *Acta Crystallogr.* **1965**, *18*, 17.
(28) Artioli, G.; Pavese, A.; Bellotto, M.; Collins, S. P.; Lucchetti, G. *Am. Miner.*, submitted.
(29) Fuoss, P. H.; Eisenberger, P.; Warburton, W. K.; Bienenstock, A. *Phys. Rev. Lett.* **1981**, *46*, 1537.
(30) Waseda, Y. Novel Application of Anomalous (Resonance) X-ray Scattering for Structural Characterization of Disordered Materials. *Lect. Notes Phys.* **1984**, 204.
(31) Allmann, R.; Jepsen, H. P. *Neues Jahrb. Mineral., Monatsh.* **1969**, 544.
(32) Hernandez-Moreno, M. J. H.; Ulibarri, M. A.; Rendon, J. L.; Sema, C. J. *Phys. Chem. Miner.* **1985**, *12*, 34.
(33) Treacy, M. M. J.; Newsam, J. M.; Deem, M. W. *Proc. R. Soc. London* **1991**, *433*, 499.
(34) Greaves, C.; Thomas, M. *Acta Crystallogr. B* **1986**, *B42*, 51.
(35) Saalfeld, H.; Wedde, M. *Z. Kristallogr.* **1974**, *139*, 129.

JP960039J